

# RSC Advances



This is an *Accepted Manuscript*, which has been through the Royal Society of Chemistry peer review process and has been accepted for publication.

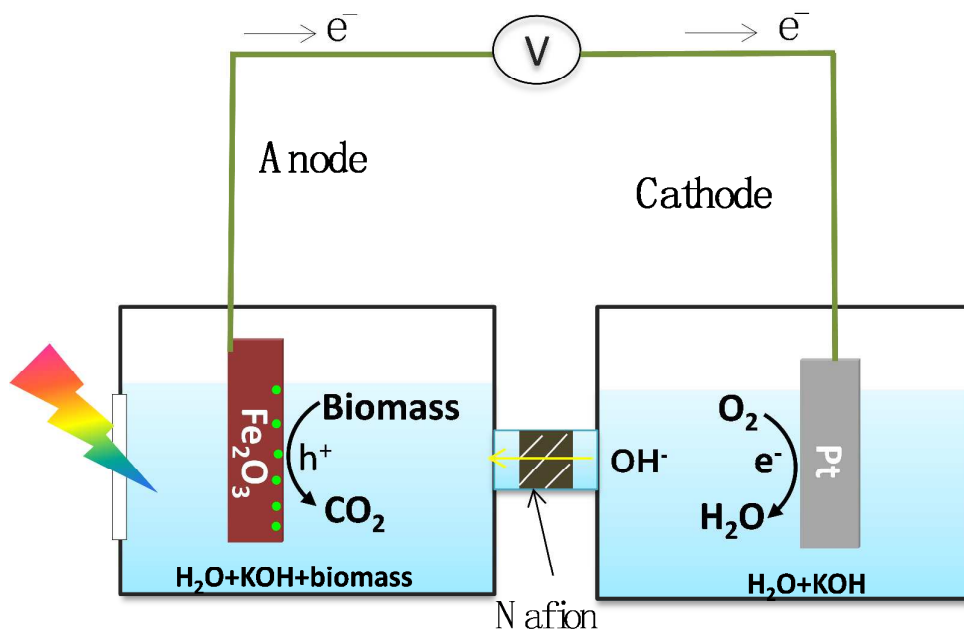
*Accepted Manuscripts* are published online shortly after acceptance, before technical editing, formatting and proof reading. Using this free service, authors can make their results available to the community, in citable form, before we publish the edited article. This *Accepted Manuscript* will be replaced by the edited, formatted and paginated article as soon as this is available.

You can find more information about *Accepted Manuscripts* in the [Information for Authors](#).

Please note that technical editing may introduce minor changes to the text and/or graphics, which may alter content. The journal's standard [Terms & Conditions](#) and the [Ethical guidelines](#) still apply. In no event shall the Royal Society of Chemistry be held responsible for any errors or omissions in this *Accepted Manuscript* or any consequences arising from the use of any information it contains.

## Abstract

Photofuel cells have been demonstrated to be a promising strategy for generating electricity using biomass. Here we present a photofuel cell with a visible light  $\alpha$ - $\text{Fe}_2\text{O}_3$  based photoanode that can be directly powered by varieties of biomasses, such as methanol, glycerol, glucose, cellulose and starch. The photocurrent density and power density of the photofuel cell are significantly enhanced by loading cocatalyst (metal hydroxide, e.g.  $\text{Ni}(\text{OH})_2$ ) on the  $\alpha$ - $\text{Fe}_2\text{O}_3$  photoanode. The power density of the photofuel cell powered by glucose is enhanced over two times, from  $0.082 \text{ mA cm}^{-2}$  for  $\alpha$ - $\text{Fe}_2\text{O}_3$  to  $0.18 \text{ mW cm}^{-2}$  for  $\text{Ni}(\text{OH})_2/\alpha$ - $\text{Fe}_2\text{O}_3$  photoanode.



1 **Transition Metals (Ni, Fe, and Cu) Hydroxides Enhanced  $\alpha$ -Fe<sub>2</sub>O<sub>3</sub>**  
2 **Photoanode-based Photofuel Cell**

3

4 Ruifeng Chong,<sup>a</sup> Zhiliang Wang,<sup>a</sup> Jun Li, Hongxian Han, Jingying Shi and Can Li\*

5

6 **Affiliations:**

7 State Key Laboratory of Catalysis, Dalian Institute of Chemical Physics, Chinese

8 Academy of Sciences, Dalian National Laboratory for Clean Energy, 457 Zhongshan

9 Road, Dalian, 116023, China.

10

11 <sup>a</sup>These authors contributed equally to this work.

12 \*To whom all correspondence should be addressed. Email: [canli@dicp.ac.cn](mailto:canli@dicp.ac.cn)

13 <http://www.canli.dicp.ac.cn>

14 Tel: 86-411-84379070 Fax: 86-411-84694447

15

16

17

18

19

20

21

## 1 Introduction

2 The utilization of abundant biomass as an energy source can prevent environmental  
3 pollution and reduce the dependence on fossil resource.<sup>1, 2</sup> The technological  
4 challenge is to sustainably capture the biomass energy using green process. Direct  
5 alcohol fuel cells (DAFCs) with potentials of high power density and pollution-free,  
6 offer a possible solution to this problem.<sup>3, 4</sup> Although DAFCs powered by low  
7 molecular weight alcohols (usually methanol or ethanol) have been demonstrated to  
8 be practically feasible, biomass-derived compounds such as glucose, polysaccharide,  
9 and cellulose have not been reported as fuels for DAFCs. This is due to the low  
10 activity of catalysts in the activation of the C–C bonds and oxidation of biomass at  
11 low temperatures.<sup>5, 6</sup> Biofuel cells can be powered by various biomasses at low  
12 temperatures; however, low electric power output, limited lifetime and rigorous  
13 reaction conditions seriously hinder their applications.<sup>7, 8</sup>

14 Photofuel cell (PFC) mainly consists of a semiconductor photoanode, a cathode,  
15 electrolyte and fuels.<sup>9-14</sup> With PFC technology, biomass as fuel can be oxidized on  
16 photoanode under light irradiation and oxygen is reduced on counter electrode  
17 through an external circuit, generating electricity. In essence, PFC is different from  
18 fuel cells reported previously, and it widens the range of biomass fuels for electricity  
19 generation. As it has been proved, various biomasses such as glycerol, glucose,  
20 saccharides, proteins, ammonia, *etc.* can be used as fuels for PFCs with TiO<sub>2</sub>  
21 photoanode. Previous work demonstrates that PFCs can convert biomass into  
22 electricity at ambient, even at low temperatures. However, TiO<sub>2</sub> and WO<sub>3</sub> with band

1 gaps of 3.2 eV and 2.8 eV, respectively, only use a small proportion of solar  
2 irradiation.<sup>15</sup> Thereby, semiconductors with wide range of light absorption are highly  
3 desired for PFCs.

4 Hematite ( $\alpha$ -Fe<sub>2</sub>O<sub>3</sub>) with optical band gap of 2.1 eV is a promising material for  
5 photoanode, due to its abundance, ecofriendly, and photochemical stability in basic  
6 electrolytes.<sup>16-18</sup> But the short excited state lifetime (~1 ps) and the small hole  
7 diffusion length (~2 to 4 nm) of hematite significantly hinder its efficiency in charge  
8 separation and collection. To overcome these problems, various strategies have been  
9 adopted, including reducing the size,<sup>19,20</sup> doping<sup>21-23</sup> and loading cocatalyst<sup>24-26</sup>, *etc.*  
10 Among them, loading cocatalyst is the most efficient way for photoelectrochemical  
11 water splitting. However,  $\alpha$ -Fe<sub>2</sub>O<sub>3</sub> loaded with appropriate cocatalyst which can  
12 distinctly enhance biomass oxidation has not been reported.

13 In this work, we present a PFC with  $\alpha$ -Fe<sub>2</sub>O<sub>3</sub> based photoanodes that directly  
14 converts biomass-derived compounds, such as methanol, glucose, glycerol, cellulose,  
15 and starch. To improve the PFC efficiency and the stability of  $\alpha$ -Fe<sub>2</sub>O<sub>3</sub> photoanode,  
16 transition metal hydroxides Ni(OH)<sub>2</sub>, Fe(OH)<sub>3</sub>, and Cu(OH)<sub>2</sub> are loaded as biomass  
17 oxidation cocatalysts. It was found that the cocatalysts can remarkably enhance the  
18 photoresponse and stability of bare  $\alpha$ -Fe<sub>2</sub>O<sub>3</sub> for biomass oxidation, which  
19 demonstrates an example for prompting PFC by loading efficient cocatalyst on  
20 photoanode.

## 21 **Experimental**

## 22 **Materials**

1 All chemicals were analytical grade and were used as purchased. Solutions were  
2 prepared using high purity water (Millipore Milli-Q purification system, resistivity >  
3 18 M $\Omega$ ·cm). The FTO (fluorine-doped tin oxide) conductive glass was purchased  
4 from Nippon Sheet Glass Company 5 (Japan) and was ultrasonic cleaned with acetone,  
5 ethanol and deionized water for 20 min each in sequence prior to use.

#### 6 **Preparation of the Fe<sub>2</sub>O<sub>3</sub> films**

7  $\alpha$ -Fe<sub>2</sub>O<sub>3</sub> films were deposited on a F-doped SnO<sub>2</sub> (FTO) substrate electrode using a  
8 modified chemical bath deposition method reported in elsewhere.<sup>27</sup> Specifically, 0.2  
9 mol L<sup>-1</sup> FeCl<sub>3</sub> (FeCl<sub>3</sub>·6H<sub>2</sub>O,  $\geq$  99%, Shanghai Chemical) aqueous solution (10 mL)  
10 and 0.3 mol L<sup>-1</sup> NH<sub>2</sub>CONH<sub>2</sub> (98%, Shanghai Chemical) were mixed in a 50 mL glass  
11 beaker and heated at 100 °C for 4 h. FTO was placed vertically in these beaker with  
12 the conducting edge facing the wall of the beaker. After the reaction, the film formed  
13 on FTO was thoroughly rinsed in high purity water and annealed at 500 °C for 3 h to  
14 get the desired phase. Finally, the prepared sample was further annealed at 750 °C for  
15 10 min.

#### 16 **Fabrication of M(OH)<sub>x</sub>/Fe<sub>2</sub>O<sub>3</sub> photoanode**

17 Ni(OH)<sub>2</sub> was deposited onto  $\alpha$ -Fe<sub>2</sub>O<sub>3</sub> by a successive ionic layer adsorption and  
18 reaction method. In a typical synthesis,  $\alpha$ -Fe<sub>2</sub>O<sub>3</sub> electrodes were dipped into 0.1 mol  
19 L<sup>-1</sup> Ni(NO<sub>3</sub>)<sub>2</sub> ( $\geq$  98.5%, Shanghai Chemical) solution for 40 s, following by drying  
20 with compressed air. Then the electrodes were dipped into 1 mol L<sup>-1</sup> KOH solution for  
21 another 40 s and dried with compressed air. And then the prepared sample was

1 washed with ethanol and dried at 60 °C for 1 h in air. Fe(OH)<sub>3</sub>/α-Fe<sub>2</sub>O<sub>3</sub> and  
2 Cu(OH)<sub>2</sub>/α-Fe<sub>2</sub>O<sub>3</sub> samples were prepared by the same method without further heat  
3 treatment

#### 4 **Characterizations of the electrodes**

5 The prepared samples were characterized by X-ray powder diffraction (XRD) on a  
6 Rigaku D/Max-2500/PC powder diffractometer using Cu Kα radiation (operating  
7 voltage: 40 kV, operating current: 20 mA, scan rate: 5° min<sup>-1</sup>). The UV–visible diffuse  
8 reflectance spectra were recorded on a UV-visible spectrophotometer (JASCO V-550)  
9 and calibrated by Kubelka-Munk method. The morphologies of the electrodes were  
10 examined by a Quanta 200 FEG scanning electron microscope (SEM) equipped with  
11 an energy dispersive spectrometer (accelerating voltage of 20 kV). Transmission  
12 electron microscopy (TEM) images were taken on a Tecnai G<sup>2</sup> Spirit (FEI company)  
13 using an accelerating voltage of 120 kV. High-resolution transmission electron  
14 microscopy (HRTEM) images were performed on Tecnai G<sup>2</sup> F30 S-Twin (FEI  
15 company) with an accelerating voltage of 300 kV. The liquid products quantitative  
16 analysis was carried out using HPLC (Agilent 1200) with refractive index (RI)  
17 detector and ultraviolet (UV, λ=210 nm) detector for arabinose, erythrose,  
18 glyceraldehyde, glycolaldehyde, glycollate and formate. Reactant and products were  
19 separated through an ion exclusion column (Alltech OA-1000) heated at 55 °C. The  
20 eluent was a solution of H<sub>2</sub>SO<sub>4</sub> (0.005 mol L<sup>-1</sup>). Products were identified by  
21 comparison with standard samples, which were obtained from Sigma–Aldrich.

#### 22 **Photoelectrochemical and electrochemical measurements**

1 All the photoelectrochemical measurements were carried out in a three-electrode cell  
2 with a flat quartz window to facilitate illumination of the photoelectrode surface. The  
3 working electrode is  $\alpha$ -Fe<sub>2</sub>O<sub>3</sub>, and Hg/HgCl<sub>2</sub> (saturated KCl) and Pt plate (2 cm × 4  
4 cm) were used as reference and counter electrode, respectively. A Nafion membrane  
5 was used to prevent the crossover between the anode and cathode. The illumination  
6 source was a 300 W Xe arc lamp and the light intensity at the surface of the electrodes  
7 was 300 mW cm<sup>-2</sup>. The electrochemical measurements were performed on a CHI  
8 760D electrochemical workstation (CHI, Shanghai) at room temperature. The  
9 electrolyte is 1 mol L<sup>-1</sup> KOH solution with/without 0.025 mol L<sup>-1</sup> glucose (or  
10 methanol (10 vol%), glycerol (0.025 mol L<sup>-1</sup>), cellulose (0.025 mol L<sup>-1</sup>) and starch (1  
11 wt%).

12 A photofuel cell was constructed using a two-compartment quartz cell with a  
13 Nafion membrane as separator.  $\alpha$ -Fe<sub>2</sub>O<sub>3</sub> and Ni(OH)<sub>2</sub>/ $\alpha$ -Fe<sub>2</sub>O<sub>3</sub> photoanodes were  
14 used as anodes and a Pt wire was used as cathode, while a Nafion membrane was  
15 served as separator. The distance between the anode and cathode is 10 cm. The  
16 photovoltaic performance of the cells was measured with a Keithley 2400 source  
17 measure unit, irradiated by AM 1.5 (100 mW cm<sup>-2</sup>).

18 The energy efficiency (PEC) and fill factor (FF) of such a device can be estimated  
19 through Equation (1) and Equation (2), respectively.

$$20 \text{ PEC} = P_{\text{Out}} / P_{\text{hv}} \times 100\% \quad (1)$$

$$21 \text{ FF} = (V_{\text{max}} \times I_{\text{max}}) / (V_{\text{oc}} \times I_{\text{sc}}) \quad (2)$$

22  $P_{\text{Out}}$  and  $P_{\text{hv}}$  represent the output electrical power and the input photochemical



1 energy, respectively;  $I_{sc}$  is the measured short circuit current; and  $V_{oc}$  is the specified  
2 open current voltage.  $I_{max}$  and  $V_{max}$  correspond to the current and voltage at the  
3 maximum power point.

#### 4 **Results and Discussions**

5 The XRD patterns of  $Fe_2O_3$  film was shown in Fig. 1a. The sample shows  
6 diffraction peaks with  $2\theta$  at  $35.6^\circ$  and  $64.0^\circ$ , which correspond to the indices of (110),  
7 and (300) planes (PDF NO. 840306) of hematite phase. The UV-Visible spectrum (Fig.  
8 1b) gives the bands of  $\alpha-Fe_2O_3$  at 410 nm and around 600 nm, which corresponds to  
9 the direct transition of  $O^{2-} 2p \rightarrow Fe^{3+} 3d$  and the transition of the spin-forbidden  $Fe^{3+}$   
10  $3d \rightarrow 3d$ , respectively.<sup>28</sup> Fig. 1c and 1d illustrate the top-view analysis and  
11 morphology of  $\alpha-Fe_2O_3$  film characterized by SEM. The film is consisted of  $\alpha-Fe_2O_3$   
12 nanorod particles, with the diameter of 20-30 nm and the length of 60-100 nm. The  
13 cross analysis of the film shows a thickness of about 300 nm with a uniform and  
14 continuous morphology.

15 Fig. 2 shows the dark and photocurrent densities of an  $\alpha-Fe_2O_3$  photoanode under  
16 light illumination. The dark response is negligible up to 0.6 V vs. SCE for both 1 mol  
17  $L^{-1}$  KOH electrolyte and 1 mol  $L^{-1}$  KOH containing glucose. Above 0.6 V vs. SCE, an  
18 anodic current formed due to water or glucose oxidation. It suggested that  $\alpha-Fe_2O_3$   
19 photoanode has equal oxidation ability for glucose and water under these conditions.  
20 Whereas in KOH, the onset potential is shifted to -0.43 V vs. SCE and the  
21 photocurrent is due to water oxidation. When glucose is added to aqueous KOH  
22 electrolyte, the photo-onset potential shifts to a lower value of -0.6 V vs. SCE and the

1 photocurrent density obviously increases. These results indicate that glucose is  
2 preferentially oxidized over water, and more photo-generated electrons and holes are  
3 used for O<sub>2</sub> reduction and glucose oxidation. The results also suggest that  $\alpha$ -Fe<sub>2</sub>O<sub>3</sub>  
4 photoanode can efficiently oxidize biomass in photochemical process, which means  
5 that the sunlight utilization for PFC could be extended to the visible light region.

6 To improve the activity and stability of  $\alpha$ -Fe<sub>2</sub>O<sub>3</sub> photoanode, transition metal  
7 hydroxides Ni(OH)<sub>2</sub>, Fe(OH)<sub>3</sub>, and Cu(OH)<sub>2</sub> were deposited on  $\alpha$ -Fe<sub>2</sub>O<sub>3</sub> film by a  
8 successive ionic layer adsorption and reaction method. The SEM elemental mapping  
9 was carried out to detect the state of the Ni(OH)<sub>2</sub> modifying on Fe<sub>2</sub>O<sub>3</sub>. As shown in  
10 Fig. S1, Ni is distributed randomly on Fe<sub>2</sub>O<sub>3</sub> and the mass ratio of Ni to Fe is ca. 0.24  
11 detected by EDS. To further study the microstructure of Ni(OH)<sub>2</sub>/ $\alpha$ -Fe<sub>2</sub>O<sub>3</sub>, HRTEM  
12 analyses were conducted. HRTEM images of a representative Ni(OH)<sub>2</sub>/ $\alpha$ -Fe<sub>2</sub>O<sub>3</sub>  
13 photoanode are shown in Fig. 3a and 3b. The HRTEM image confirms the Ni species  
14 present on the edge of  $\alpha$ -Fe<sub>2</sub>O<sub>3</sub>. The magnified HRTEM image in Fig. 3b exhibits  
15 fringes with lattice spacing of *ca.* 0.37 nm, which corresponds to the (012) plane of  
16  $\alpha$ -Fe<sub>2</sub>O<sub>3</sub>. While the lattice fringes with a spacing of 0.218 and 0.154 nm is consistent  
17 with the (103) and (300) planes of the 3Ni(OH)<sub>2</sub>•2H<sub>2</sub>O ( $\alpha$ -Ni(OH)<sub>2</sub>). The EDS  
18 linescan performed across the  $\alpha$ -Fe<sub>2</sub>O<sub>3</sub> nanorod shows the distinct spatial profiles of  
19 Fe and Ni, confirming Ni species being deposited on Fe<sub>2</sub>O<sub>3</sub> surface (Fig. S2, ESI<sup>†</sup>).  
20 These results reveal that  $\alpha$ -Ni(OH)<sub>2</sub> nanoparticles adhere to the surface of  $\alpha$ -Fe<sub>2</sub>O<sub>3</sub>,  
21 forming heterojunctions between the two components.

Fig. 4a shows the linear sweep voltammetric (LSV) curves of  $\alpha$ -Fe<sub>2</sub>O<sub>3</sub> and

Ni(OH)<sub>2</sub>/α-Fe<sub>2</sub>O<sub>3</sub> photoanode in 1 mol L<sup>-1</sup> KOH electrolyte with glucose under chopped light illumination. After loading Ni(OH)<sub>2</sub> cocatalyst, the photocurrent for glucose oxidation on the α-Fe<sub>2</sub>O<sub>3</sub> electrode is significantly increased. The Ni(OH)<sub>2</sub> film itself shows no photoresponse for glucose oxidation (Fig. S3, ESI†). While in 1 mol L<sup>-1</sup> KOH electrolyte without glucose, the photocurrent curve of Ni(OH)<sub>2</sub>/α-Fe<sub>2</sub>O<sub>3</sub> electrode is different from that of α-Fe<sub>2</sub>O<sub>3</sub> electrode (Fig. S4, ESI†), which may be due to the oxidation of Ni(OH)<sub>2</sub> in the photoelectrochemical process. This suggests that Ni(OH)<sub>2</sub> acts as the active site for glucose oxidation.

The enhanced photocurrent observed for the Ni(OH)<sub>2</sub>/α-Fe<sub>2</sub>O<sub>3</sub> sample in Fig. 4b is possibly due to that Ni(OH)<sub>2</sub> traps photo-generated holes, forming Ni<sup>3+</sup> species, then efficiently catalyze the glucose oxidation, and simultaneously Ni<sup>3+</sup> is reduced back to Ni<sup>2+</sup>.<sup>29-33</sup> Namely, the cocatalyst Ni(OH)<sub>2</sub> can enhance the photo-generated charges separation of α-Fe<sub>2</sub>O<sub>3</sub> and provide the catalytic sites for glucose oxidation.

Some metal components (Fe and Cu) with the multiple oxidation states were demonstrated to be excellent electrocatalysts for glucose sensor.<sup>34,35</sup> So, Fe(OH)<sub>3</sub> and Cu(OH)<sub>2</sub> were also used to modify α-Fe<sub>2</sub>O<sub>3</sub> photoanode for glucose oxidation. As shown in Figs. 4c and 4d, The major phenomenological observation is that modification of α-Fe<sub>2</sub>O<sub>3</sub> with Fe(OH)<sub>3</sub> and Cu(OH)<sub>2</sub> can also obviously enhance the photocurrent density. The above results show that Fe(OH)<sub>3</sub> and Cu(OH)<sub>2</sub> play the similar role to that of Ni(OH)<sub>2</sub>. Namely, they can also improve the hole transfer from Fe<sub>2</sub>O<sub>3</sub> to glucose and provide active sites for glucose oxidation.

The α-Fe<sub>2</sub>O<sub>3</sub> based photoanodes with cocatalysts, like Ni(OH)<sub>2</sub> reported in this

study can photooxidize various biomass molecules in combination with an  $O_2$ -reducing cathode. Fig. 5 shows the photocurrent density generated by methanol, glycerol, cellulose and starch. The photocurrent densities of  $Ni(OH)_2/\alpha-Fe_2O_3$  photoanodes can reach 4.7 and 5.0  $mA\ cm^{-2}$  at 0 V vs. SCE fueled by methanol and glycerol, respectively. Whereas cellulose and starch with relative big molecular weight, give photocurrent densities respectively about 4.0 and 3.5  $mA\ cm^{-2}$  at 0 V vs. SCE with  $Ni(OH)_2/\alpha-Fe_2O_3$  photoanodes. It was noted that photocurrent density produced by starch was lower than that obtained from cellulose solution under similar conditions, probably because of the slow hydrolysis of starch. The results illustrate that all these biomass materials are promising fuels for PFC and loading cocatalyst is an efficient method for improving the PFC performance.

A simple PFC consisting of  $\alpha-Fe_2O_3$  (or  $Ni(OH)_2/\alpha-Fe_2O_3$ ) photoanode and Pt plate cathode in glucose solution were fabricated. Fig. 6 illustrates the voltage-current density and power density-current density curves, and Table 1 displays the photovoltaic parameters for both PFCs. The device with  $\alpha-Fe_2O_3$  photoanode yields an open-circuit voltage ( $V_{oc}$ ) of 0.38 V, a short-circuit current ( $I_{sc}$ ) of 1.17  $mA\ cm^{-2}$ , and a fill factor (FF) of 0.18, resulting in an overall power conversion efficiency (PCE) of 0.082%. In contrast, the photovoltaic device containing the  $Ni(OH)_2/\alpha-Fe_2O_3$  photoanode presents  $V_{oc}$  of 0.43 V, the  $I_{sc}$  of 1.97  $mA\ cm^{-2}$  and FF of 0.21. As a result, the  $Ni(OH)_2/\alpha-Fe_2O_3$  based cell reaches a conversion efficiency of 0.18%, outperforming that of the  $Fe_2O_3$ -based device. As shown in power density-current density curves, the device with  $\alpha-Fe_2O_3$  photoanode yields a

maximum power density of  $0.082 \text{ mA cm}^{-2}$ , while the maximum power density ( $P_{\text{max}}$ ) of  $\text{Ni(OH)}_2/\alpha\text{-Fe}_2\text{O}_3$  is  $0.18 \text{ mA cm}^{-2}$ . These results reveal that with  $\alpha\text{-Fe}_2\text{O}_3$  based PFC, biomass can be directly converted into electrical energy and the efficiency of can be enhanced by modifying  $\alpha\text{-Fe}_2\text{O}_3$  photoanode with cocatalysts.

The stability of  $\alpha\text{-Fe}_2\text{O}_3$  based photoanodes and the intermediates in the reaction were tested in  $1 \text{ mol L}^{-1}$  KOH electrolyte containing glucose. Fig. 7 illustrates the amperometric  $I-t$  curves of  $\alpha\text{-Fe}_2\text{O}_3$  and  $\text{Ni(OH)}_2/\alpha\text{-Fe}_2\text{O}_3$  electrodes under continuous illumination at  $0 \text{ V vs. SCE}$ . The photocurrent of bare  $\alpha\text{-Fe}_2\text{O}_3$  after 4 h illumination is 86% of the initial value, but in the case of  $\text{Ni(OH)}_2/\alpha\text{-Fe}_2\text{O}_3$  electrode the photocurrent can be maintained by 96%. Additionally, XPS results (Fig. S5, ESI†) shows that the valence state of Ni are maintained during the reaction in 4 h, suggesting that  $\text{Ni}^{2+}$  in  $\text{Ni(OH)}_2/\alpha\text{-Fe}_2\text{O}_3$  electrode can be rapidly regenerated. It suggests that cocatalyst is rather effective for improving the steady state of  $\alpha\text{-Fe}_2\text{O}_3$  photoanode.

The products from glucose with  $\text{Ni(OH)}_2/\alpha\text{-Fe}_2\text{O}_3$  photoanode was detected by HPLC after 6 h reaction. These intermediates are identified as arabinose, erythrose, glyceraldehyde, glycolaldehyde, glycollate and formate, and the carbon balance is ca. 71% (Table S1 and Fig. S6, ESI†). The carbon loss of 29% is mainly attributed to the release of  $\text{CO}_2$ , which are produced from the cleavage of C-C bond of glucose and its derivatives. The result implies that  $\alpha\text{-Fe}_2\text{O}_3$  based photoanodes can efficiently cleave the C-C bond in biomass and oxidize it to  $\text{CO}_2$  in the PFC at low temperature.

## Conclusion

The PFCs consisting of  $\alpha$ -Fe<sub>2</sub>O<sub>3</sub> based photoanode and an O<sub>2</sub>-reducing cathode was fabricated. The sunlight utilization of PFCs was extended to the visible light region. We firstly reported that transition metal hydroxides (Ni, Fe and Cu) are excellent cocatalysts of  $\alpha$ -Fe<sub>2</sub>O<sub>3</sub> for biomass oxidation. The performance of PFC can be obviously enhanced by loading these cocatalysts on  $\alpha$ -Fe<sub>2</sub>O<sub>3</sub> photoanode. Moreover, compared with traditional DAFCs, PFCs can efficiently break the C-C bond of the biomass, and thus PFCs can be directly powered with natural biomass molecules.

## Acknowledgments

This work is financially supported by the National Natural Science Foundation of China (NSFC, grant No. 21090340, 21373209).

## References

1. P. McKendry, *Bioresource Technol.*, 2002, **83**, 37-46.
2. J. Potočník, *Science*, 2007, **315**, 810-811.
3. E. Antolini, *ChemSusChem*, 2013, **6**, 966-973.
4. E. H. Yu, U. Krewer and K. Scott, *Energies*, 2010, **3**, 1499-1528.
5. A. Serov and C. Kwak, *Appl. Catal. B: Environ.*, 2010, **97**, 1-12.
6. A. Brouzgou, A. Podias and P. Tsiakaras, *J. Appl. Electrochem.*, 2013, **43**, 119-136.

7. S. D. Minter, B. Y. Liaw and M. J. Cooney, *Curr. Opin. Biotechnology*, 2007, **18**, 1-7.
8. F. Ahmad, M. N. Atiyeh, B. Pereira and G. N. Stephanopoulos, *Biomass Bioenerg.*, 2013, **56**, 179-188.
9. M. Kaneko, J. Nemoto, H. Ueno, N. Gokan, K. Ohnuki, M. Horikawa, R. Saito and T. Shibata, *Electrochem. Commun.*, 2006, **8**, 336-340.
10. R. L. Chamousis and F. E. Osterloh, *ChemSusChem*, 2012, **5**, 1-7.
11. P. J. Barczuk, A. Lewera, K. Miecznikowski, P. Kulesza and J. Augustynskiz, *Electrochem. Solid St.*, 2009, **12**, B165-B166.
12. M. Antoniadou, D. Kondarides, DiamantoulaLabou, S. Neophytides and PanagiotisLianos, *Sol. Energy Mat. Sol. C.*, 2010, **94**, 592-597.
13. M. Antoniadou and P. Lianos, *Catal. Today*, 2009, **144**, 166-171.
14. Y. Yan, J. Fang, Z. Yang, J. Qiao, Z. Wang, Q. Yu and K. Sun, *Chem. Commun.*, 2013, **49**, 8632-8634.
15. S. D. Tilley, M. Cornuz, K. Sivula and M. Grätzel, *Angew. Chem. Int. Ed.*, 2010, **49**, 6405-6408.
16. K. Sivula, F. Le Formal and M. Grätzel, *ChemSusChem*, 2011, **4**, 432-449.
17. D. A. Wheeler, G. Wang, Y. Ling, Y. Li and J. Z. Zhang, *Energy Environ. Sci.*, 2012, **5**, 6682-6702.
18. K. Sivula, R. Zboril, F. Le Formal, R. Robert, A. Weidenkaff, J. Tucek, J. Frydrych and M. Grätzel, *J. Am. Chem. Soc.*, 2010, **132**, 7436-7444.
19. S. K. Mohapatra, S. E. John, S. Banerjee and M. Misra, *Chem. Mater.*, 2009, **21**, 3048-3055.
20. J. Zhu, Z. Yin, D. Yang, T. Sun, H. Yu, H. E. Hoster, H. H. Hng, H. Zhang and Q. Yan, *Energy Environ. Sci.*, 2013, **6**, 987-993.
21. S. Saremi-Yarahmadi, K. G. U. Wijayantha, A. A. Tahir and B. Vaidhyanathan, *J. Phys. Chem. C*, 2009, **113**, 4768-4778.
22. I. Cesar, A. Kay, J. A. G. Martinez and M. Grätzel, *J. Am. Chem. Soc.*, 2006, **128**, 4582-4583.
23. Y. Hu, A. Kleiman-Shwarsctein, A. J. Forman, D. Hazen, J. Park and E. W. McFarland, *Chem. Mater.*, 2008, **20**, 3803-3805.
24. S. D. Tilley, M. Cornuz, K. Sivula and M. Grätzel, *Angew. Chem. Int. Ed.*, 2010, **49**,

- 6405-6408.
25. I. Cesar, A. Kay, J. A. G. Martinez and M. Grätzel, *J. Am. Chem. Soc.*, 2006, **128**, 4582-4583.
  26. J. Y. Kim, G. Magesh, D. H. Youn, J. Jang, J. Kubota, K. Domen and J. S. Lee, *Sci. Rep.*, 2013, **3**, 2681.
  27. F. Lin and S. Boettcher, *Nat. Mater.*, 2014, **13**, 81-86.
  28. P. R. Martins, M. A. Rocha, L. Angnes, H. E. Toma and K. Araki, *Electroanal.*, 2011, **23**, 2541-2548.
  29. J. Nai, S. Wang, Y. Bai and L. Guo, *Small*, 2013, **9**, 3147-3152.
  30. S. Xie, T. Zhai, W. Li, M. Yu, C. Liang, J. Gan, X. Lu and Y. Tong, *Green Chem.*, 2013, **15**, 2434-2440.
  31. S. Xie, T. Zhai, W. Li, M. Yu, C. Liang, J. Gan, X. Lu and Y. Tong, *Green Chem.*, 2013, **15**, 2434-2440.
  32. X. Cao and N. Wang, *Analyst*, 2011, **136**, 4241-4246.
  33. S. Sun, X. Zhang, Y. Sun, S. Yang, X. Song and Z. Yang, *Appl. Mater. Interfaces*, 2013, **5**, 4429-4437.



## Figures and Tables

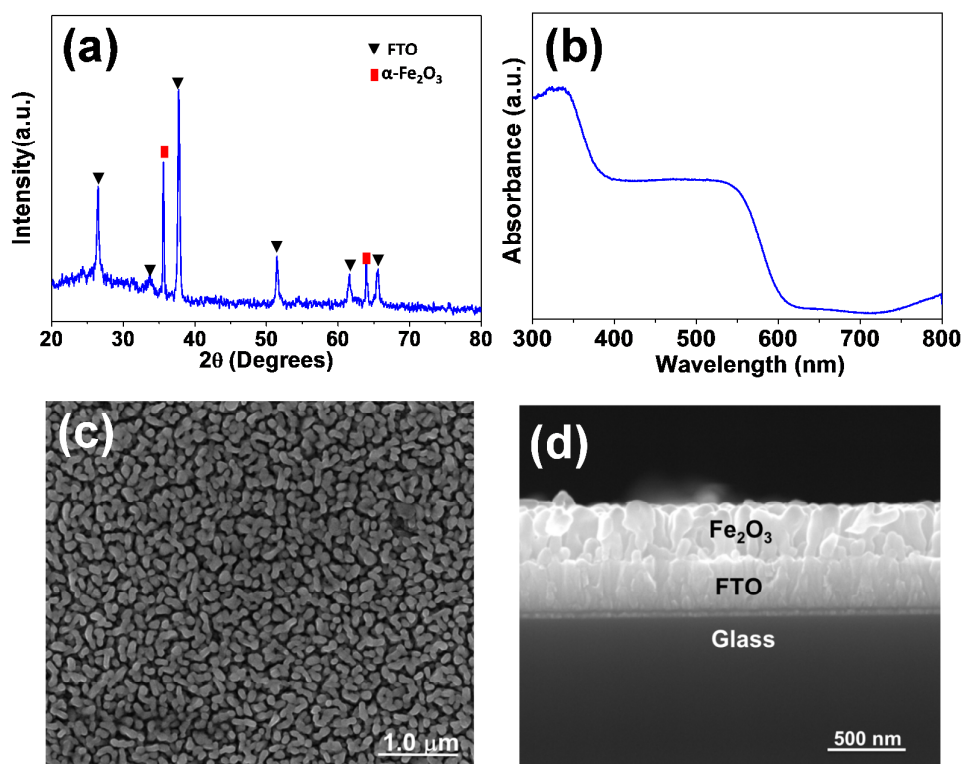


**Fig. 1** (a) XRD pattern and (b) UV-vis absorption spectra of of Fe<sub>2</sub>O<sub>3</sub> film. (c) Top view and (d) side view SEM images of Fe<sub>2</sub>O<sub>3</sub> film.

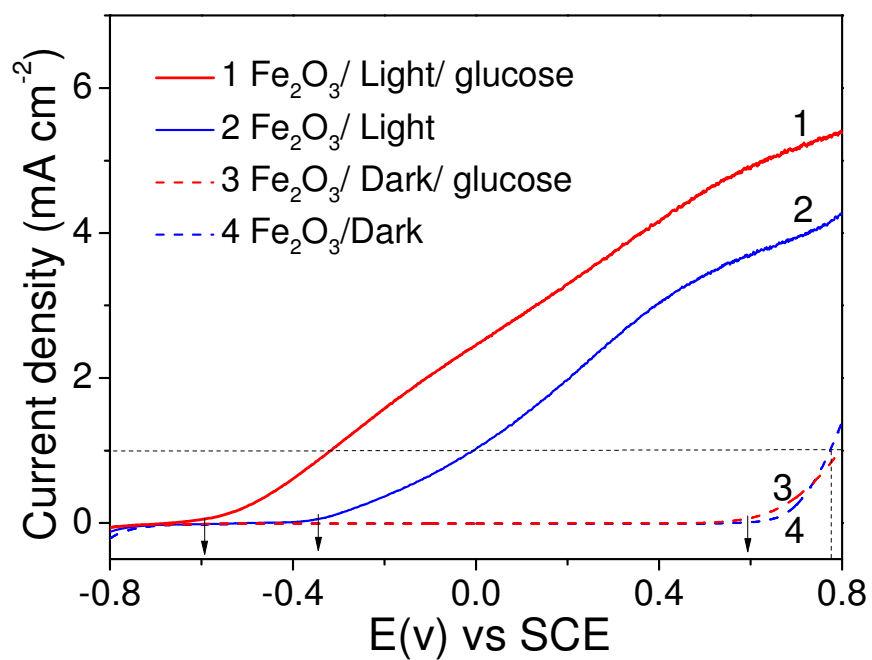


**Fig. 2** Dark and photocurrent densities for  $\alpha$ -Fe<sub>2</sub>O<sub>3</sub> photoanode in 1 mol L<sup>-1</sup> KOH electrolyte and in 1 mol L<sup>-1</sup> KOH electrolyte containing 0.025 mol L<sup>-1</sup> glucose; Light source: 300 W Xe lamp; Scanning rate: 20 mV s<sup>-1</sup>.

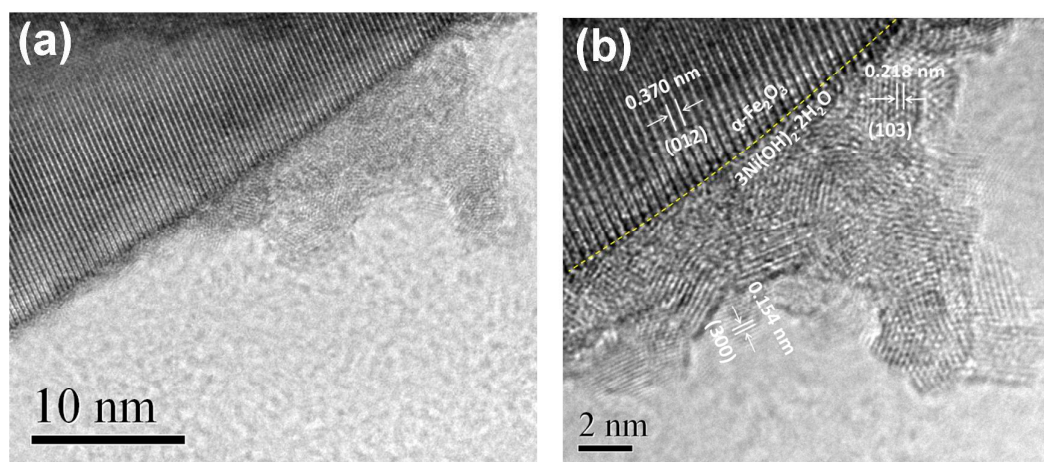


**Fig. 3** (a) HRTEM image of  $\text{Ni(OH)}_2/\alpha\text{-Fe}_2\text{O}_3$  and (b) the magnified HRTEM image of the selected frame from image (a).

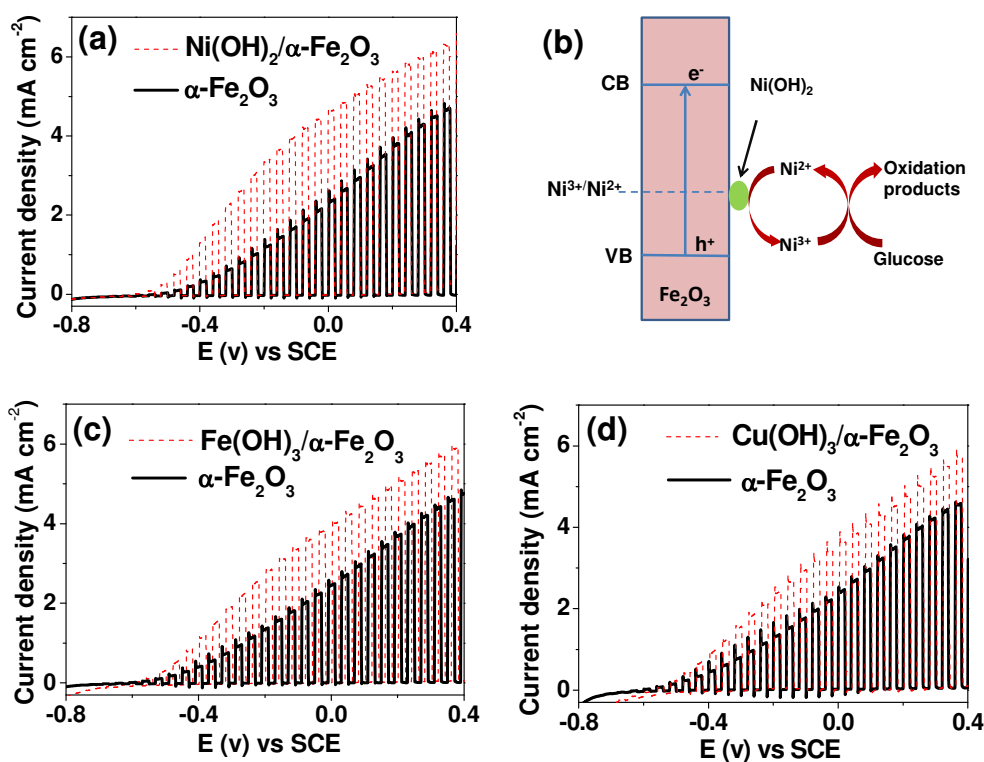


**Fig. 4** (a) LSV curves of  $\text{Fe}_2\text{O}_3$  and  $\text{Ni(OH)}_2/\alpha\text{-Fe}_2\text{O}_3$  photoanodes under chopped light illumination; (b) The possible process of glucose oxidation over  $\text{Ni(OH)}_2/\text{Fe}_2\text{O}_3$  photoanode; (c) and (d) LSV curves of  $\alpha\text{-Fe}_2\text{O}_3$  photoanodes modified with  $\text{Fe(OH)}_3$  and  $\text{Cu(OH)}_2$ ; Reaction condition:  $1 \text{ mol L}^{-1}$  KOH aqueous solution with  $0.025 \text{ mol L}^{-1}$  glucose; Light source: 300 W Xe lamp; Scanning rate:  $20 \text{ mV s}^{-1}$ .

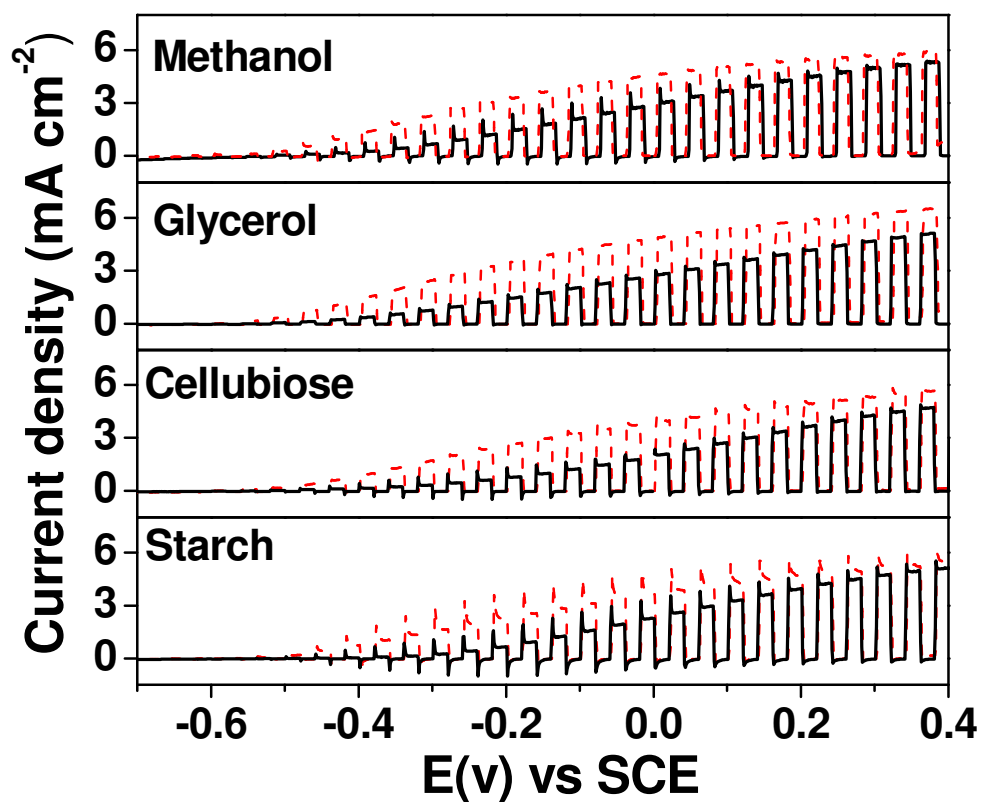


**Fig. 5** LSV curves of  $\alpha\text{-Fe}_2\text{O}_3$  (solid) and  $\text{Ni(OH)}_2/\alpha\text{-Fe}_2\text{O}_3$  (dashed) photoanodes in  $1 \text{ mol L}^{-1}$  KOH electrolyte with different biomass-derived compounds under chopped light illumination; methanol (10 vol%); glycerol ( $0.025 \text{ mol L}^{-1}$ ); cellubiose ( $0.025 \text{ mol L}^{-1}$ ) and starch (1 wt%). Light source: 300 W Xe lamp; Scanning rate:  $20 \text{ mV s}^{-1}$ .

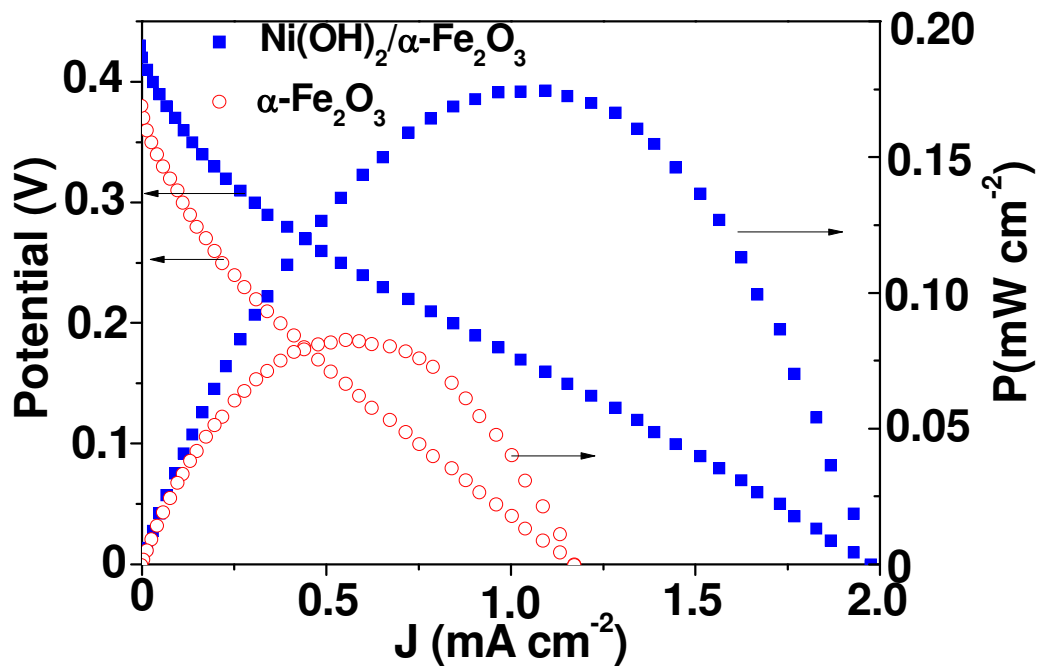


**Fig.6** I-V and I-P curves of PFCs for  $\alpha\text{-Fe}_2\text{O}_3$  and  $\text{Ni(OH)}_2/\alpha\text{-Fe}_2\text{O}_3$  photoanodes operating with light irradiation of in  $1 \text{ mol L}^{-1}$  KOH electrolyte containing  $0.025 \text{ mol L}^{-1}$  glucose, under irradiation with the AM 1.5G simulated solar light ( $100 \text{ mW}\cdot\text{cm}^{-2}$ ).

**Table 1** Photovoltaic parameters of the light-assisted glucose fuel cells consisting of  $\alpha\text{-Fe}_2\text{O}_3$  and  $\text{Ni(OH)}_2/\alpha\text{-Fe}_2\text{O}_3$  photoanodes.

Anode	Intensity ( $\text{mW cm}^{-2}$ )	$V_{\text{OC}}$ (V)	$I_{\text{SC}}$ ( $\text{mA cm}^{-2}$ )	FF	P ( $\text{mW cm}^{-2}$ )	PEC (%)
-------	--------------------------------------	------------------------	--	----	------------------------------	------------

---

$\alpha\text{-Fe}_2\text{O}_3$	100	0.38	1.17	0.18	0.082	0.08
$\text{Ni(OH)}_2/\alpha\text{-Fe}_2\text{O}_3$	100	0.43	1.98	0.21	0.18	0.18

*See in Fig.6 for the test condition.*

---

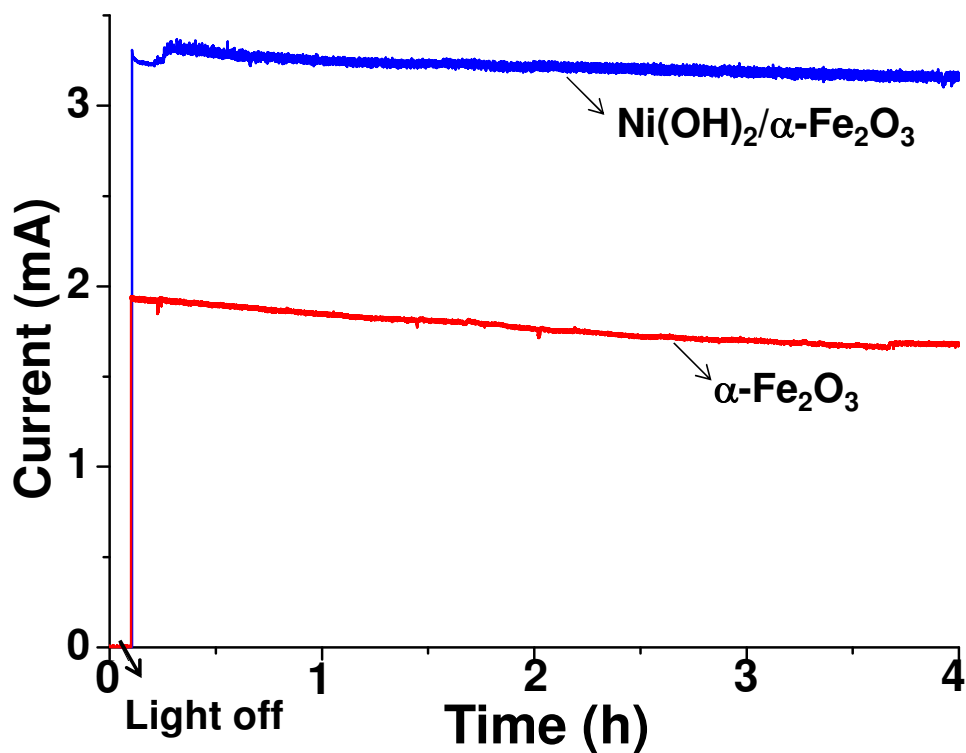


**Fig. 7** Amperometric I-t curves of  $\alpha\text{-Fe}_2\text{O}_3$  and  $\text{Ni(OH)}_2/\alpha\text{-Fe}_2\text{O}_3$  photoanodes at 0 V vs. SCE in a  $1 \text{ mol L}^{-1}$  KOH electrolyte containing  $0.025 \text{ mol L}^{-1}$  glucose. Light source: 300 W Xe lamp. The area of  $\alpha\text{-Fe}_2\text{O}_3$  film is  $1.58 \text{ cm}^2$ .

